Nuclear Instruments and Methods in Physics Research B 540 (2023) 227–233

Contents lists available at ScienceDirect

Nuclear Inst. and Methods in Physics Research, B

journal homepage: www.elsevier.com/locate/nimb

Preliminary results from a study of luminescent materials—For application in the beam imaging system at the ESS

R.J.W. Frost [a,b,*], C.A. Thomas [c], M. Elfman [b], R. Johansson [c], M. Hartl [c], H. Kocevar [c], K. Michel [c], S. Joshi [d], S. Björklund [d]

[a] Department of Physics and Astronomy, Uppsala University, Uppsala, Sweden
[b] Department of Physics, Lund University, Lund, Sweden
[c] Accelerator Division, European Spalation Source (ESS), Lund, Sweden
[d] Department of Engineering Science, University West, Trollhätten, Sweden

ARTICLE INFO

Keywords:
ESS
Beam imaging
Luminescent screens
Chromia alumina
YAG

ABSTRACT

As part of the development of the beam imaging system at the European Spallation Source, luminescent screens have been fabricated by the flame spraying of scintillating materials onto stainless steel backings. A total of seven screens were produced, three of chromia alumina (Al_2O_3:Cr), two of YAG ($Y_3Al_5O_{12}$:Ce) and two of a 50/50 mix of these. The properties of these screens under proton irradiation were evaluated using a 2.55 MeV proton beam at currents of up to 10 μA. Irradiation times were up to 25 h per sample, during which luminescence-, spectrographic-, thermal- and current-data was sampled at a rate of 1 Hz. Preliminary results of these measurements are reported here; with a quantitative analysis presented for one of the chromia alumina screens and a qualitative comparison of all three material types. The luminescent yield for chromia alumina was determined to be around 2000 photons/MeV for a virgin screen, and was found to drop to 1.5% after 167 mC of proton irradiation. A recovery of the luminescence of chromia alumina to >60% was observed after beam current was reduced for an 8 h period. Observations indicate that the YAG and mixed composition screens retain higher luminescence than the chromia alumina even at temperatures of over 200 °C. It is indicated that the luminescence from YAG feeds the R-lines of chromia alumina in the mixed composition screens.

1. Introduction

One of the challenges presented by the high-power ion beams used for neutron spallation is the level of control required to limit damage to the target and other associated infrastructure. This level of control can be partly achieved by means of imaging the power-density distribution of the beam at key locations. The European Spallation Source [1] will deliver a pulsed 2 GeV proton beam [2], with and average power of 5 MW; each pulse being raster scanned over a fixed are on the target. As such, the beam imaging system used [3–6] must be capable of providing quantitative information in an automated manner, so that the beam can be quickly shut down should irregularities be detected. Scintillating screens are frequently used in the diagnostic systems of particle accelerators [7], but for such a system to be deployed at ESS, suitable luminescent materials have to be identified and qualified. Two common choices of luminescent material [8] are chromia alumina (Al_2O_3:Cr) and YAG ($Y_3Al_5O_{12}$:Ce). These materials have been used to fabricate stainless-steel scintillation screens at ESS, which were then flame-sprayed at University West. The present work is part of an ongoing project to qualify these screens for use in the high-power beam imaging system.

The qualification of screen materials for the type of application described above, includes gaining a detailed understanding of a wide range of properties. Luminescence yield, for example, is a crucial parameter that will influence many of the properties of the optical and acquisition system; but is on its own insufficient, as luminescent yield is known to be a function of temperature. The stainless steel of the ESS target wheel is expected to reach operational temperatures of 250–350 °C, and at these temperatures the light output from the ruby lines given by chromia alumina drops by more than 50%. In addition to this, the resistance of the scintillating materials to high radiation-dose is important, as radiation damage will introduce defects and vacancies that can trap the excited states required to generate luminescence. A knowledge of how luminescence yield changes with dose must therefore be obtained before defining the longevity of the system. With further regards to the acquisition and interpretation of luminescence data, spectral information also becomes important. All

* Corresponding author at: Department of Physics and Astronomy, Uppsala University, Uppsala, Sweden.
E-mail address: rob.frost@physics.uu.se (R.J.W. Frost).

https://doi.org/10.1016/j.nimb.2023.04.015
Received 1 November 2022; Received in revised form 16 March 2023; Accepted 14 April 2023
Available online 5 May 2023

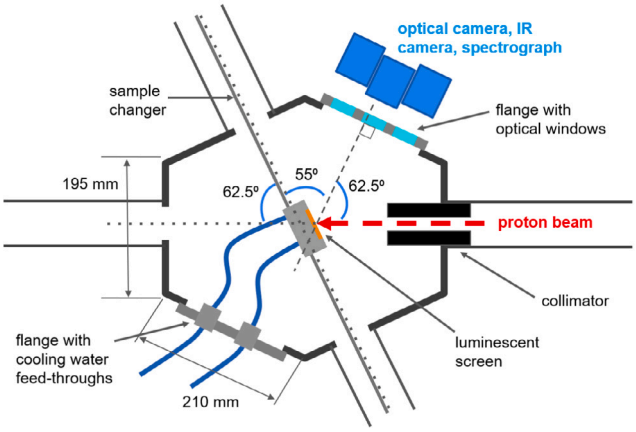

Fig. 1. Schematic representation of the experimental setup used for the irradiation of the luminescent screens. Key dimensions and angles are indicated. The diagram is not to scale.

these factors affect the light output of a given screen under given irradiation conditions, but in addition to these, there must also be study of properties such as the luminescent lifetime [9], thermo-mechanical resistance to beam impact, and control of the industrial production process [10].

In this study, the luminescent-, thermal- and spectra-properties of specially prepared chromia alumina, YAG and a mixed composition screens, were investigated under irradiation with a proton beam at 2.55 MeV. The primary aim of the study was to determine the luminescent yield (photons/MeV), and how it degrades with accumulating radiation dose, this being critical to understand how the imaging system for the beam on target at the ESS will perform during operation. Technical aspects of the experiment are present here in detail, along with preliminary results obtained on the properties of these screens. A more comprehensive treatment of the data will be published later, in combination with data obtained in other works.

2. Experimental setup

Measurements on chromia alumina and YAG scintillating screens, under proton irradiation, were conducted at Nuclear Applications Laboratory, Lund University. The screens were produced as part of a trial for testing the flame-spraying parameters of these materials [10]. All screens were produced on stainless-steel discs, 10 mm thick and 25 mm diameter. Powders used to produce the screens were specially developed at ESS; making sure, for example, that the grain sizes were between 5 and 60 μm in diameter. The flame spraying of the powders onto the screen backings was conducted at University West. Seven of the final screens produced with the optimised spraying parameters, which presented the expected luminescence properties, were selected for irradiation. The luminescent screens were irradiated, using a 2.55 MeV proton-beam of up to 10 μA, generated by a 3 MV single ended Pelletron accelerator from NEC. A schematic of the measurement chamber used is shown in Fig. 1. Post irradiation photographs of each screen can be seen in Fig. 2, where the dark spots show the areas that have been irradiated by the proton beam.

Each screen was mounted to a water-cooled sample holder, positioned at the centre of the measurement chamber, with the face of the screen at 27.5° to the normal of the incident beam. The exposed surface of each screen was a circular area, 25 mm in diameter, this being much larger than the size limit of the beam, restricted by a 10 mm diameter collimator. In practice, focusing of the beam was used to create a beam-spot on the screens. The optical measurement of the beam, demonstrated in Fig. 3, reports RMS sizes of about 1.3 mm × 2.1 mm. All Screens were irradiated separately. Composition,

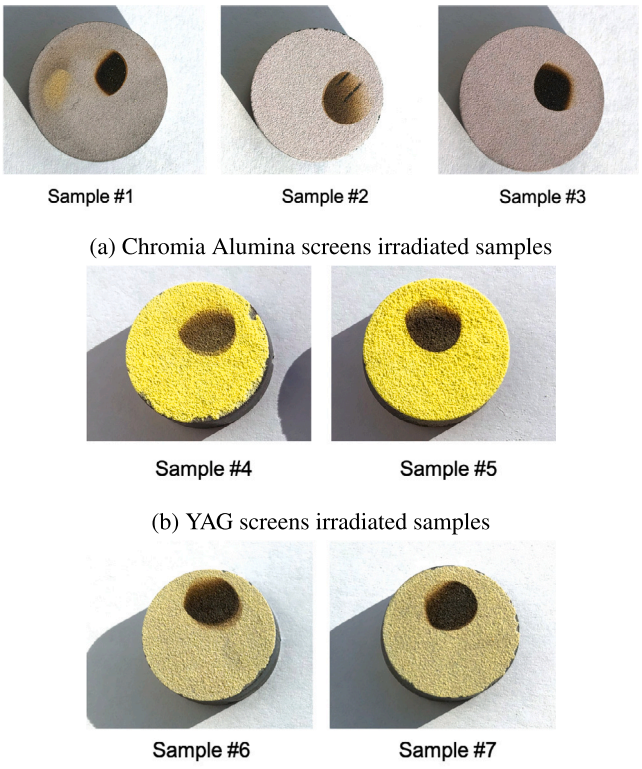

Fig. 2. Photos of the irradiated sample screens.

thickness and measurement time for each screen is summarised in Table 1. Measurement of the sample thicknesses was performed with a capaNCDT 6200 capacitive thickness sensor, with high resolution in the 0–1 mm range, from Micro-epsilon [11].

Luminescent and thermal data was acquired using: a Mako-234G optical camera from Allied Vision [12], with a model MVL12M23, 12 mm F/1.4 lens from Thorlabs [13]; a model A35 infrared camera from FLIR [14]; and two spectrographs, models CCS100 and CCS200, from Thorlabs. All measurement equipment was positioned outside of the chamber and viewed the screen under irradiation through three view ports: two with quartz windows for the optical camera and the spectrograph; and the third with a ZnSe window for the infrared camera. The choice of window materials was made to ensure flat transmission in the working range of wavelengths. All windows were provided by Thorlabs. The exposure time of the optical camera was chosen so that the total yield from a virgin-screen was set at 3/4 of the cameras 12 bit range. This ensured the largest dynamic range possible for the experiment.

Beam-current measurement was taken from both the experimental chamber and the sample holder. Both of these were electrically isolated from the beamline and all other equipment. The current was read using a 414 A analogue picoammeter from Keithley Instrumentation [15], with a 0–10 V output calibrated to 10 μA at full range. This analogue output was digitised by a 4262 picoscope from Pico Technology [16]. The sampling of the current was made at 10 kS/s, acquiring 9900 samples within a 0.99 s window, with a pretrigger time of 0.495 s relative to an external input trigger which was delivered to all instruments. The external trigger had a frequency of 1 Hz, and was provided by a 4064 signal generator from B&K Precision [17].

All instrumentation was driven and read by an ESS developed implementation of the areaDetector plugin [18,19] for EPICS. The data for each trigger signal was saved by means of the h5 plugin that recorded data from each instrument, including meta data, such as time exposure

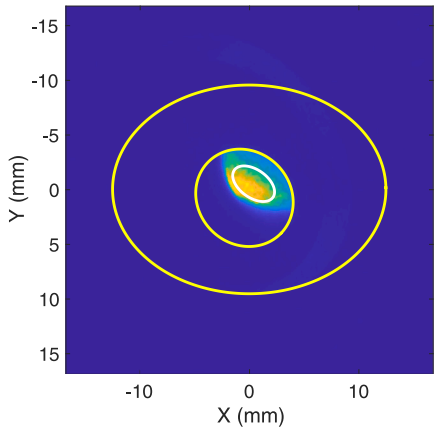

Fig. 3. Beam on Sample #3 as seen by the optical camera. The image has been rotated and analysed to extract the beam RMS sizes (white ellipse), and to scale these according to the measured dimensions of the screen size (larger yellow circle) and collimator size (smaller yellow circle).

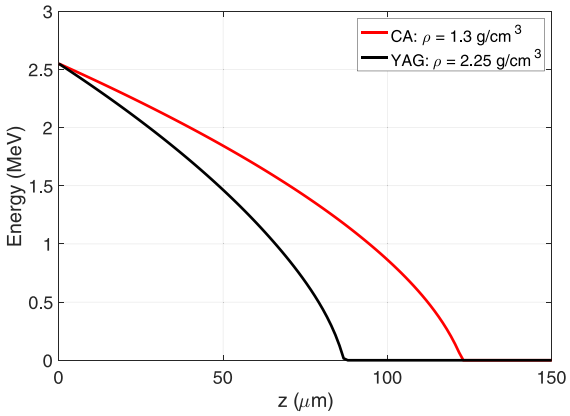

Fig. 4. Proton energy lost along the depth of the screen material, calculated from SRIM model. For references to colour, the reader is referred to the online version of the article. Note the density for CA is measured, whereas for YAG is has been estimated.

Table 1
Summary of the luminescent screens irradiated in this work. For 'composition', CA = Al_2O_3:Cr, YAG = $Y_3Al_5O_{12}$:Ce and Mix = a 1:1 mixture of the two.

Sample reference	Composition	Thickness (μm)	Measurement time (h)
1	CA	54 ± 6	20
2	CA	70 ± 1	24
3	CA	83 ± 1	24
4	YAG	197 ± 3	24
5	YAG	154 ± 2	24
6	Mix	142 ± 14	24
7	Mix	123 ± 1	21

for the camera and the spectrograph, gain, calibration factor, etc; the PROC plugin was used for the IR camera in order to deliver images with Celsius look up table.

3. Results and discussion

3.1. Scope of the analysis presented

Over the course of the 161 h of measurement time used in this study, 5 TB of data was generated. Here, a selection of key results, with preliminary analysis thereof, are presented. The discussion in this report focuses largely on Sample #3 as an example of the results obtained for all chromia alumina samples. Due to assumptions that must be made on the energy deposited in the YAG and mixed composition screens (discussed in Section 3.2), a comprehensive analysis of these data has not yet been performed. This said, conclusions are drawn where reasonable on the properties and performance of all three materials studied. A full treatment of the data collected, in combination with additional results from the broader study of these luminescent materials, is to be published elsewhere [10].

3.2. Energy deposition and sample heating

Fig. 4 shows the energy loss of the proton beam as predicted by SRIM [20]. In order to calculate the energy loss, the sample density must be known; the densities used in these calculation being shown in the figure legend. For the chromia alumina samples, the density has been measured; for the YAG however, density measurement has not yet been performed and an estimation is therefore used as input for the SRIM calculation. This estimate is based on the relative mass of material in the feed for the flame coating process, and the final screen thickness, of the YAG screens in comparison to the chromia alumina screens. Verification of this estimation will be performed in future work, but until this is undertaken, the predicted energy loss for YAG shown in Fig. 4 should be used with caution.

The thicknesses of the samples produced, vary between 50 μm and 200 μm. Hence, most if not all of the beam energy is deposited in the screen material. This has two consequences. Firstly, the material can be strongly heated, which biases the luminescence yield measurement as this is temperature dependent; and secondly, when comparing the efficiency of the screens, the total amount of energy deposited per proton is a normalising factor. An accurate knowledge of the screen density and thickness is therefore critical. Previous measurements with the chromia alumina screens [10] showed the yield of the R-lines to drop 50% between room temperature and 230 °C, but the total yield to reduce by only 10%. This measurement is yet to be performed on the YAG and mixed-composition screens, however, similar behaviour is expected. As this is the temperature range anticipated for the ESS target, the temperature correction to the yield is considered to be second order when compared to the degradation induced by the radiation dose. In the present work, it is therefore important that the screens are kept within this temperature range by cooling, and that the temperature is monitored using the IR camera to ensure this is the case.

The design of the cooling system was shown to be sufficient to remove most of the heat from the screens during irradiation. This was validated by the thermo-mechanical modelling in ANSYS, of an 100 μm thick chromia alumina layer on a stainless steel backing; similar to Sample #3. These simulations showed that for a Gaussian beam of $\sigma_x = \sigma_y = 5$ mm, a temperature of >400 °C would be reached in the absence of cooling. With a simulated cooling system removing 1 W, temperature in the screen was predicted to reach only 60 °C and 30 °C for 10 μA and 1 μA beam current respectively; these current corresponding to power densities of 1 kW/cm^3 and 0.25 kW/cm^3 in the sample respectively. These values can be compared to those shown in Fig. 5. Fig. 5(a) shows an IR image of Sample #3 at the beginning of irradiation. The temperature of the sample can be seen to be no higher than 65 °C with a 7 μA beam current. Fig. 5(b) shows the beam current and temperature of Sample #3 over the full irradiation time. The variation seen in the ratio of beam current to temperature, at different stages of irradiation, is due to variation of the beam profile and hence the current density. Further discussion on the beam profile is given in Section 3.4. It should be noted that, despite the effectiveness of the cooling system with regard to the thinner, chromia alumina screens, it displayed limits for the thicker YAG screens where equilibrium temperature reached over 200 °C.

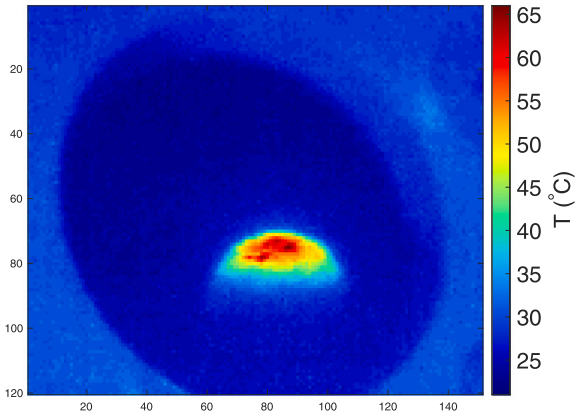

(a) Image of Sample #3 from the IR camera, at the beginning of the irradiation. The proton-beam current is 7 μA and peak temperature of the sample is around 65°C.

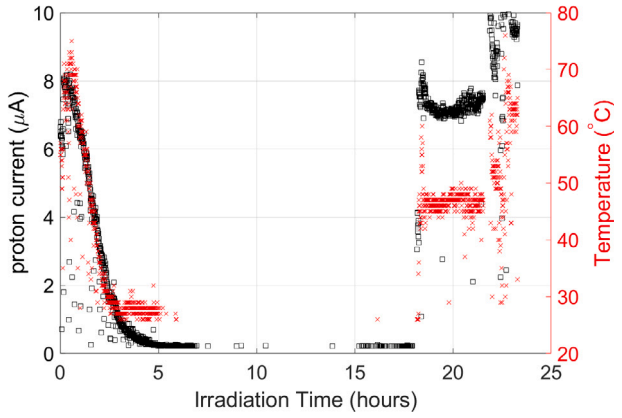

(b) Beam current incident on Sample #3 (left axis); and temperature of Sample #3 (right axis); over the full course of irradiation.

Fig. 5. Sample #3 irradiation: the temperature of the chromia alumina is recorded during the irradiation, together with the beam current. For any measured current less than 0.2 μA, the current data is in the noise level and hence has not been analysed. This seen as the amount of data becomes sparse in (a), particularly in the 7–15 h region.

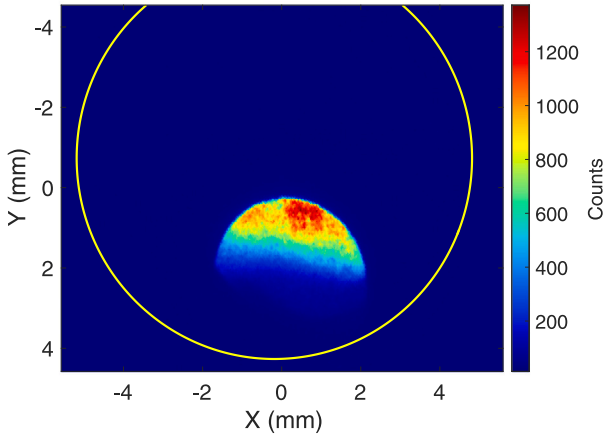

(a) Image of the beam on Sample #3 from the optical camera at the same time as Fig. 5a. The yellow ellipse shows the fit to outer circle of the sample holder, used to determine the beam size.

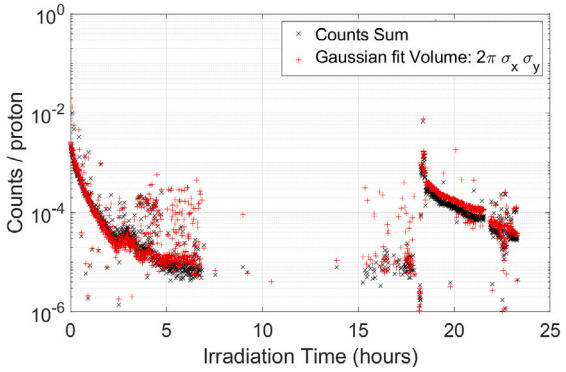

(b) Luminescence of Sample #3 in counts per proton, during the irradiation period, evaluated by two different methods. The beam current corresponding to these data is shown in Fig. 5b.

Fig. 6. Sample #3 irradiation: the luminescence of the chromia alumina is recorded during the irradiation; the beam current can be read from Fig. 5(b). For any measured current less than 0.2 μA, the current data is in the noise level and hence has not been analysed. This seen as the amount of data becomes sparse in (a), particularly in the 7–15 h region.

3.3. Luminescent yield of chromia alumina

Fig. 6(a) shows the optical image of Sample #3, corresponding to the IR image in Fig. 5(a). The yellow ellipse fitted to the outer circle of the sample holder is as described in Section 2, with reference to Fig. 3. It was from such optical images that the luminescent-yield data was extracted. Fig. 6(b) shows the luminescence as measured on the optical-camera images, over the full course of sample irradiation. The plot represents the yield in counts per proton. The total number of counts is evaluated by two means: a simple sum of the counts less the background counts, and a 2D-Gaussian fit, that returns beam size, position, intensity and orientation of the main axis of the fitted 2D-Gaussian. The agreement between the two calculation methods permits confidence in the result. Further analysis and data curing is needed to refine these data, however, this preliminary result is sufficient to draw initial conclusions; and to move forward with the processing of the luminescent data for the other screens, which will be reported elsewhere.

Following the experiment, the optical camera was tested using a known light source incident on a material of known transmittance, in the exact optical configuration with regards to lens settings, exposure time and solid angle. From this test it was possible to obtain a value for the number of photons-per-count in the camera image; this being 1.6×10^6. Hence, for the fresh chromia alumina screen analysed, a total yield of 3200 photons/proton was obtained. Sample #3 is ~80 μm thick, and as such, 2.55 MeV protons lose on average 1.5 MeV whilst travelling through it. This results in a value for luminescence for the chromia alumina of ~2000 photons/MeV; approximately six times higher than that obtained by Simon et al. [21] but consistent with previous results obtained by the authors [10]. The luminescence value reported here is also comparable to the Ti-doped alumina luminescence reported by Mikhailik et al. [22]. It should be noted that the 50–70 °C temperature of the sample, impacts the measurement by causing a drop in total luminescence yield, estimated to be around 10%. This temperature dependence drop in yield has not been taken into account when deriving the luminescence yield reported above.

The total proton charge irradiating the sample is a proxy for the irradiation fluence. In Fig. 7, the normalised luminescence yield for Sample #3 is reported as function of the total proton charge. The yield after a total dose of $Q = 0.1674$C, or 1.0×10^{18} protons is 1.5% of the fresh sample; this being consistent with what is observed at the beam imaging system on the spallation target of SNS [23]. An additional,

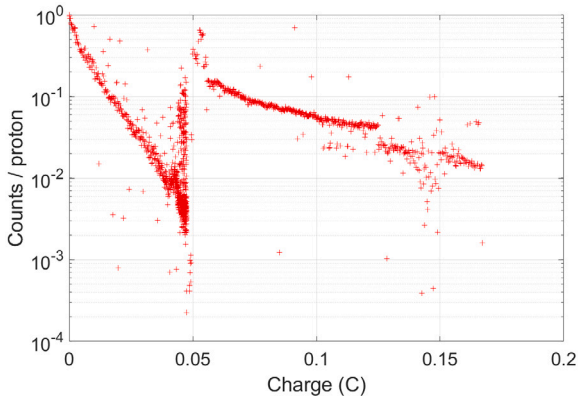

Fig. 7. Normalised luminescence-yield for Sample #3, as shown in Fig. 6(b), as function of the total proton charge, over the full course of the irradiation.

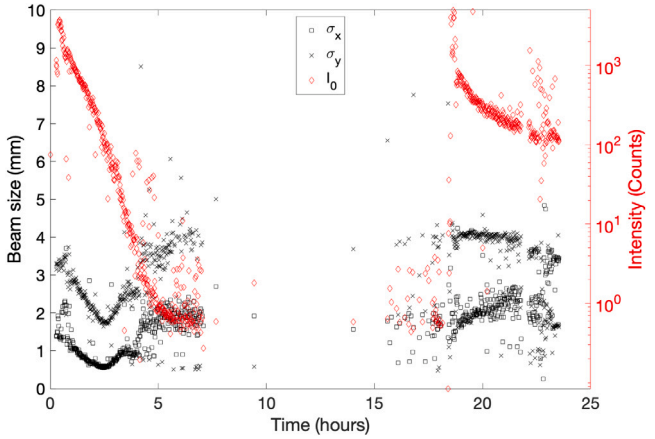

Fig. 8. RMS beam sizes in the main beam axis (σ_x and σ_y) and intensity (I_0), over the full course of the irradiation of Sample #3.

and interesting, feature in the data presented here, arises due to the significant drop in beam current during the middle of the experiment: The luminescence curve in Fig. 7 presents a jump after the low current irradiation from 6 h to 18 h, with the normalised yield returning to 66% of the value given by the virgin screen. This is consistent with the apparent recovery observed in a previous irradiation campaign [10]. This relates to defects and vacancies, particularly F-centres [24,25], in the material. These defects can partially recover with temperature and time, due to the ability to migrate mm from there original sites after being produced.

It is expected that the YAG and mixed composition screens are brighter than the chromia alumina, but further analysis is required to quantify this. As an observation, the optical camera used saturates for an exposure time of between 10 ms and 20 ms when viewing the chromia alumina, whereas for the YAG and mixed composition it is between 0.1 ms and 0.5 ms. It must also be considered however, that the energy loss is estimated to be 2.5 MeV in YAG and only 1.5 MeV in the chromia alumina; the temperature of the YAG and chromia alumina is also very different, being over 200 °C and less than 70 °C for each material respectively.

An additional point of interest, is the observation of surface blackening of the irradiated area, seen in the images presented in Fig. 2. This will be investigated in future work to understand, for example, the composition and thickness of this dark layer, and the impact it may have in reducing the photon yield observed. Nonetheless, irradiation has been performed on chromia alumina in other work, with an 8 MeV proton beam, where similar degradation of the yield and similar recoveries of the yield after 8–12 h pauses was observed. There was no formation of black layer in these 8 MeV irradiations, the surface of the samples after irradiation remaining pristine.

3.4. Beam profile

A screen for high power beam imaging has to report a beam profile, for which linearity in the luminescence is critical. Although was not possible to directly measure the linearity in this irradiation experiment, some reasonable assumptions can be made, and linearity of the system is not considered to be a limiting factor. Firstly the linearity of the optical camera, from the manufactures data, is in the 0.1% range. This, coupled with the flat transmission of the optical system, means only linearity of the screen need be considered. This is the case for both the experimental instrumentation, and the instrument to be installed at ESS. With this in mind, the linearity of the system when implemented at the ESS, will be assured the fact that the luminescence can be considered constant for each beam-pulse that will be imaged, even if the yield rapidly changes with the radiation dose. This is due to a combination of the short duration of the pulses, and the raster scanning of each pulse (see Refs. [3–6] for details). It is true that the linearity of the yield can be affected in the case of very high beam density, as has been observed at European XFEL [26]. But to reach these densities, a micron size ESS beam would be required, as opposed to the cm size beam which will be use.

What was possible to measure in this experiment, was beam size, beam position and the intensity of the luminescence. All images captured by the optical camera, for Sample #3, were analysed and fitted with a 2D Gaussian function. The results for beam size and intensity, over the course of irradiation, are shown in Fig. 8. The reported RMS beam sizes were verified, by performing the same fitting procedure on the images from the IR camera and comparing the results. The two measurements were found to be consistent, over the full irradiation time. The reported beam sizes are also found to be in relation with the lattice setting of the beam line. The beam was focused on the screen and limited by a 10 mm diameter collimator. Hence, the range of RMS sizes 2–4 mm × 1–2 mm is consistent. The consistency between IR and optical beam-profiles also reinforces the idea, presented in Section 3.2, that temperature has little influence on the total intensity of the luminescence within the ranges found in this work. The position of the beam obtained by this fitting method, also shows only minor variation over the duration of measurement. The result therefore implies that shifting of the position of the beam on the screen, is a second order contribution to the variations in yield, described in Section 3.3.

3.5. Spectral analysis

Fig. 9 shows the spectrograph data collected for all seven screens, grouped in the three sub figures according to screen composition. All spectra have been normalised to a peak intensity of one, for the purpose of visualisation. The cumulative spectra are also shown in the figures, in order to show where the spectral power reside. The spectra from chromia alumina in Fig. 9(a), are characteristic for this material: with two narrow peaks (inseparable in this image) associated with R1 and R2 ruby lines at around 700 nm; and side peaks associated with vibrational luminescent modes [27–29]. Similarly, the spectra from YAG in Fig. 9(b), are characteristic: dominated by a broad distribution between 500 and 700 nm [30,31]. The mixed-composition spectra presented in Fig. 9(c) show more novel results: with the bright, broad and narrow spectra combined.

For the mixed-composition screens, nearly 50% of the power can be seen to come directly from the broad distribution of the YAG. The detailed luminescent properties of this new material have yet to be analysed, but it seems that the ruby may be enhanced by the YAG

luminescence, in addition to being driven directly by the proton energy loss. If this is the case then the lifetime under radiation could be prolonged relative to chromia alumina alone. The combination of chromia alumina and YAG is also expected to produce a typical spectrum with measurable quantities uniquely depending of temperature. The spectrum from the chromia alumina as function of temperature is well characterised, the R-line centres a linear function thereof; while the YAG spectrum is expected to behave differently with temperature to the chromia alumina spectrum. These properties can potentially be used to measure the absolute temperature of the screens and substrate with high accuracy.

4. Summary and outlook

This work is part of a wider study, into the properties of chromia alumina and YAG scintillation screens for high-power beam imaging. A selection of screens with differing thickness and compositions were irradiated with a continuous MeV proton beam. Beam current, sample temperature and light output were simultaneously recorded over irradiation times of up to 25 h for each screen; spectral data was also collected. A preliminary analysis of the large volume of data obtained has been presented. A summary of the key findings from this analysis is as follows:

- sample heating as a function of beam current for chromia alumina screens could be successfully modelled;
- the thicker YAG and mixed composition screens reached significantly higher temperatures (>200 °C) than the cromia alumina screens (<70 °C);
- a luminescence yield of ~2000 photons/MeV was obtained for fresh chromia alumina;
- the luminescence yield for chromia alumina was found to drop to ~1.5% after 167 mC of beam current;
- recovery of chromia alumina to >60% of virgin luminescence was observed after an 8 h period of low current (<0.2 μA) irradiation;
- there is indication that high temperature YAG retains a higher luminescence than chromia alumina at elevated temperature;
- fitting of beam profiles has been successfully demonstrated;
- there is indication that YAG luminescence feeds the chromia alumina R-lines in the mixed composition screens.

Although analysis of the YAG and mixed composition screens is limited in this report, the impression is that these screens seem to possess some higher performance characteristics in comparison to chromia alumina: if YAG at above 200 °C is indeed brighter than chromia alumina at room temperature, this is a huge advantage when considering applications such as the monitoring of beam on target; and if it can be proven that the spectrum of mixed composition screens permits absolute temperature measurement, then this would also be an extremely useful diagnostic tool. A more detailed analysis is required however, before any firm conclusions can be drawn with regards to these points. In addition to a more comprehensive analysis of the data collected here, further work is to include:

- density measurements on YAG:Ce and mixed composition screens, so that accurate values for energy deposition in these materials can be obtained;
- the collection of data from post irradiation examination of the screens, including electron microscopy and X-ray diffraction.

All of the screens studied in this work are potentially good candidates for high-power beam imaging systems, as they show a spectrum in the visible range and are therefore compatible with standard camera technology. The fact that the new chromia alumina material, produced at ESS and sprayed at University West, is comparable to qualified material such as the one used at SNS, brings this new screen material closer to qualification for use in the ESS beam-imaging system.

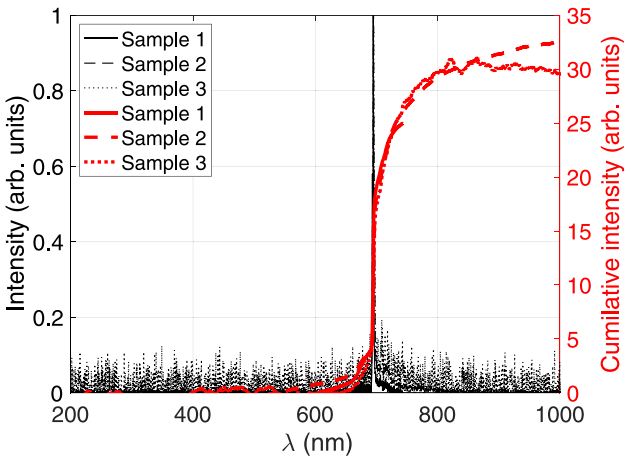

(a) chromia alumina.

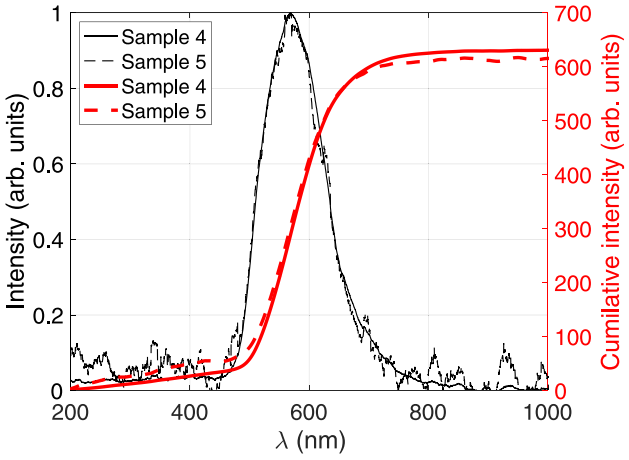

(b) YAG.

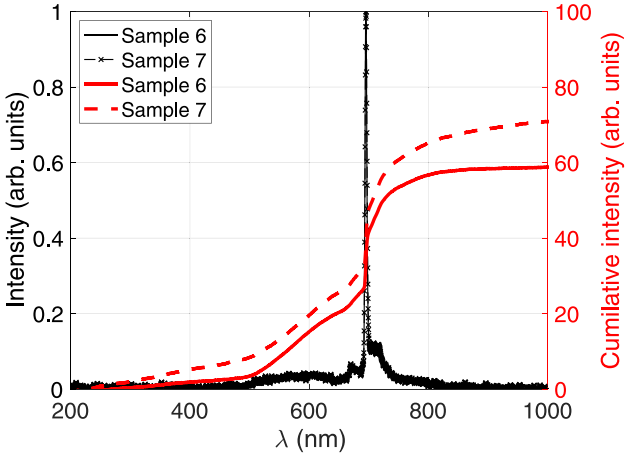

(c) Mixed composition.

Fig. 9. Spectra (black) and cumulative spectra (red), recorded for all seven screens during proton irradiation.

Declaration of competing interest

The authors declare that they have no known competing financial interests or personal relationships that could have appeared to influence the work reported in this paper.

Acknowledgements

The authors would like to give thanks, collectively, to the ESS diagnostics group, the ESS controls group and the ESS manufacturing workshop; for the broad range of contributions they have made to this project.

References

[1] European Spallation Source ERIC, Box 176, SE-221 00, Lund, Sweden, URL https://europeanspallationsource.se.
[2] H. Thomsen, S. Møller, The beam delivery system of the European Spallation Source, in: Proc. of 57th ICFA Advanced Beam Dynamics Workshop on High-Intensity and High-Brightness Hadron Beams, JACoW, 2016, pp. 427–432, http://dx.doi.org/10.18429/JACoW-HB2016-WEAM7Y01.
[3] M. Göhran, R. Linander, T. Grandsaert, T. Shea, C. Thomas, Proton beam imaging options for the ESS target, in: Proc. 5th International Particle Accelerator Conference (IPAC'14), JACoW, 2014, pp. 3659–3661, http://dx.doi.org/10.18429/JACoW-IPAC2014-THPME168.
[4] M. Donna, T. Grandsaert, M. Göhran, R. Linander, T. Shea, Optical system for ESS target protection, in: Proc. of 3rd International Beam Instrumentation Conference (IBIC2014), JACoW, 2015, pp. 389–392.
[5] M. Ibison, et al., Optical system design for the ESS proton beam and target diagnostics, in: Proc. of 7th International Particle Accelerator Conference (IPAC'16), JACoW, 2016, pp. 347–349, http://dx.doi.org/10.18429/JACoW-IPAC2016-MOPMR043.
[6] M. Ibison, C. Welsch, E. Adli, H. Gjersdal, G. Christoforo, T. Shea, C. Thomas, D. Naeem, Development of a beam imaging system for the European spallation source tuning dump, Nucl. Instrum. Methods. Phys. Res. A 950 (2020) 162790, http://dx.doi.org/10.1016/j.nima.2019.162790.
[7] B. Walasek-Höhne, G. Kube, Scintillating screen applications in beam diagnostics, in: Proc. of DIPAC2011, Hamburg, Germany, 2011, pp. 533–557.
[8] K. Renuka, W. Ensinger, C. Andre, F. Becker, P. Forck, R. Haseitl, A. Reiter, B. Walasek-Höhne, Transverse beam profile monitoring using scintillation screens for high energy ion beams, in: Proc. of BIW2012, Newport News, VA USA, 2012, pp. 183–185.
[9] C. Thomas, M. Hartl, Y. Lee, T. Shea, E. Adli, H. Gjersdal, M. Jaekel, O. Rohne, S. Joshi, Preliminary measurement on potential luminescent coating material for the ESS target imaging systems, in: Proc. of 5th International Beam Instrumentation Conference (IBIC2016), JACoW, 2017, pp. 559–562, http://dx.doi.org/10.18429/JACoW-IBIC2016-TUPG82.
[10] C. Thomas, A. Järild, E. Wiklund, T. Shea, M. Hartl, K. Michel, S. Joshi, S. Björklund, Luminescent thermal-sprayed coated screens for high power beams and targets, 2022, Manuscript in Preparation.
[11] Micro-Epsilon Measurement Technology, Königbacher Str. 15. 94496 Ortenburg, Germany, URL https://www.micro-epsilon.com.
[12] Allied Vision, Taschenweg 2a, 07646 Stadtroda, Germany, URL https://www.alliedvision.com.
[13] Thorlabs Sweden A.B., 431 35 Mölndal, Sweden, URL https://www.thorlabs.com.
[14] Teledyne FLIR LLC, FLIR Systems AB, Antennvägen 6, P.O. Box 7376, SE-187 15 Täby, Sweden, URL https://www.flir.eu.
[15] 14150 SW Karl Braun Drive, P.O. Box 500 Beaverton, OR 97077, United States, Tektronix, Inc. URL https://www.tek.com/en/products/keithley.
[16] Pico Technology, James House, Colmworth Business Park, St Neots, Cambridgeshire, PE19 8YP, United Kingdom, URL https://www.picotech.com.
[17] 22820 Savi Ranch Pkwy, Yorba Linda, CA 92887, United States, B&K Precision Corporation, URL https://www.bkprecision.com.
[18] M.L. Rivers, areaDetector: Software for 2-D detectors in EPICS, AIP Conf. Proc. 1234 (1) (2010) 51–54, http://dx.doi.org/10.1063/1.3463256.
[19] M.L. Rivers, areaDetector: EPICS software for 2-D detectors, in: Proc. of the 16th International Conference on Accelerator and Large Experimental Control Systems (ICALEPCS'17), JACoW, 2018, pp. 1245–1251, http://dx.doi.org/10.18429/JACoW-ICALEPCS2017-THDPL03.
[20] J. Ziegler, M. Ziegler, J. Biersack, SRIM – The stopping and range of ions in matter (2010), Nucl. Instrum. Methods. Phys. Res. B 268 (11) (2010) 1818–1823, http://dx.doi.org/10.1016/j.nimb.2010.02.091.
[21] C. Simon, P. Ausset, E. Bordas, J. Fils, F. Harrault, F. Leprêtre, F. Senée, Y. Serruys, O. Tuske, Scintillating screens investigations with proton beams at 30 keV and 3 MeV, in: 5th International Beam Instrumentation Conference (IBIC2016), JACoW, 2017, pp. 273–276, http://dx.doi.org/10.18429/JACoW-IBIC2016-MOPG79.
[22] V. Mikhailik, H. Kraus, M. Balcerzyk, W. Czarnacki, M. Moszyński, M. Mykhaylyk, D. Wahl, Low-temperature spectroscopic and scintillation characterisation of Ti-doped Al2O3, Nucl. Instrum. Methods. Phys. Res. A 546 (3) (2005) 523–534, http://dx.doi.org/10.1016/j.nima.2005.02.033.
[23] W. Blokland, Experience with and studies of the SNS target imaging system, in: Proc. of 3rd International Beam Instrumentation Conference (IBIC2014), JACoW, 2015, pp. 447–451.
[24] E. Kotomin, V. Kuzovkov, A. Popov, R. Vila, Kinetics of F center annealing and colloid formation in Al2O3, Nucl. Instrum. Methods. Phys. Res. B 374 (2016) 107–110, http://dx.doi.org/10.1016/j.nimb.2015.08.055.
[25] T. Yano, H. Konishi, S. Yamazaki, M.I. bin Idris, K. Yoshida, Recovery of neutron-irradiation-induced defects of Al2O3, Y2O3, and yttrium-aluminum garnet, J. Nucl. Sci. Technol. 54 (8) (2017) 891–898, http://dx.doi.org/10.1080/00223131.2017.1324330.
[26] G. Kube, A. Novokshonov, S. Liu, M. Scholz, Identification and mitigation of smoke-ring effects in scintillator-based electron beam images at the European XFEL, in: Proc. of 39th Free Electron Laser Conf., Hamburg, Germany, JACoW, 2019, pp. 301–306, http://dx.doi.org/10.18429/JACoW-FEL2019-WEB01.
[27] G. Salek, A. Devoti, E. Lataste, A. Demourgues, A. Garcia, V. Jubera, M. Gaudon, Optical properties versus temperature of Cr-doped γ - and α -Al2O3: Irreversible thermal sensors application, J. Lumin. 179 (2016) 189–196, http://dx.doi.org/10.1016/j.jlumin.2016.07.004.
[28] D. Nelson, M. Sturge, Relation between absorption and emission in the region of the R lines of ruby, Phys. Rev. 137 (4A) (1965) http://dx.doi.org/10.1103/PhysRev.137.A1117.
[29] A. Schawlow, D. Wood, A. Clogston, Electronic spectra of exchange-coupled ion pairs in crystals, Phys. Rev. Lett. 3 (6) (1959) 271–273, http://dx.doi.org/10.1103/PhysRevLett.3.271.
[30] T. Yanagida, H. Takahashi, T. Ito, D. Kasama, T. Enoto, M. Sato, S. Hirakuri, M. Kokubun, K. Makishima, T. Yanagitani, H. Yagi, T. Shigeta, T. Ito, Evaluation of properties of YAG (Ce) ceramic scintillators, IEEE Trans. Nucl. Sci. 52 (5) (2005) 1836–1841, http://dx.doi.org/10.1109/TNS.2005.856757.
[31] E. Mihóková, M. Nikl, J. Mareš, A. Beitlerová, A. Vedda, K. Nejezchleb, K. Blažek, C. D'Ambrosio, Luminescence and scintillation properties of YAG:Ce single crystal and optical ceramics, J. Lumin. 126 (1) (2007) 77–80, http://dx.doi.org/10.1016/j.jlumin.2006.05.004.